J|A|C|S ARTICLES

Published on Web 11/23/2009

Imaging Hindered Rotations of Alkoxy Species on TiO_2(110)

Zhenrong Zhang,[†] Roger Rousseau,*[,†] Jinlong Gong,[§,‡] Bruce D. Kay,[†] and Zdenek Dohnálek*[,†]

Fundamental and Computation Sciences Directorate and Institute for Interfacial Catalysis, Pacific Northwest National Laboratory, Richland, Washington 99352, and Department of Chemical Engineering, University of Texas at Austin, Austin, Texas 78712

Received September 2, 2009; E-mail: Roger.Rousseau@pnl.gov; Zdenek.Dohnalek@pnl.gov

Abstract: We present the first scanning tunneling microscopy (STM) study of the rotational dynamics of organic species on any oxide surface. Specifically, variable-temperature STM and dispersion-corrected density functional theory (DFT-D) are used to study the alkyl chain conformational disorder and dynamics of 1-, 2-, 3- and 4-octoxy on rutile TiO_2(110). Initially, the geminate pairs of the octoxy and bridging hydroxyl species are created via octanol dissociation on bridging-oxygen (O_b) vacancy defects. The STM images provide time-averaged snapshots of octoxy species rotating among multiple energetically nearly degenerate configurations accessible at a given temperature. In the calculations we find that the underlying corrugated potential energy surface is a result of the interplay between attractive van der Waals dispersion forces, leading to weak attractive C···Ti and repulsive C···O_b interactions which lead to large barriers of 50−70 kJ mol^{-1} for the rotation of the octoxy alkyl chains across the O_b rows. In the presence of the geminate hydroxyl groups we find that the relative populations of the various conformations as well as the rotational barriers are perturbed by the presence of geminate hydroxyl due to additional C···hydroxyl repulsions.

1. Introduction

The motion of adsorbed species plays an important role in many fundamentally and industrially important processes, including heterogeneous catalysis, crystal and thin-film growth, self-assembly, dissolution/precipitation, molecular motors and rotors, and others.[1−8] Unfortunately, due to the challenging nature of adsorbate dynamics studies, our understanding of diffusion and rotation of adsorbates is rather limited. Two types of ensemble-averaged techniques, infrared spectroscopy[9,10] and electron-stimulated desorption ion-angular distribution (ESDIAD),[11−13] have been previously employed to explore adsorbate rotations at surfaces. For example, on oxides, temperature-dependent changes in the vibrational−rotational spectra have been used to follow rotational motion of CH_3− groups anchored on porous surfaces of glass[9] and alumina,[10] demonstrating their free rotation about the anchoring carbon−substrate bond. Recently, our understanding of adsorbate rotational dynamics on single-crystal metal surfaces has advanced significantly, primarily due to atomically resolved imaging experiments via scanning tunneling microscopy (STM).[4−8] Here we present the first STM study of the rotational dynamics of an organic species, octoxy, on an oxide surface, TiO_2(110).

Recently, we have investigated adsorption, dissociation, and diffusion of alcohols on rutile TiO_2(110) as a model system for understanding technologically important catalytic and photocatalytic oxidation of organic contaminants on TiO_2.[14−18] We have shown that, on TiO_2(110), alcohols dissociate via O−H bond scission on the most prevalent type of surface defect site—a bridge-bonded oxygen (O_b) vacancy (O_V)—resulting in the formation of adjacent alkoxy−hydroxy (RO_b−HO_b) pairs on the same O_b row, as shown schematically in Figure 1.[16,17] Related studies demonstrated that alkoxy species diffuse via a novel O_V-assisted mechanism.[18]

In this report, we examine the rotational dynamics of the alkoxy species derived from 1-, 2-, 3-, and 4-octanol anchored by O_V on the O_b row. The long octoxy chain facilitates imaging

[†] Pacific Northwest National Laboratory.
[‡] University of Texas at Austin.
[§] Present address: Department of Chemistry and Chemical Biology, Harvard University, Cambridge, MA 02138.

(1) Kottas, G. S.; Clarke, L. I.; Horinek, D.; Michl, J. *Chem. Rev.* **2005**, *105*, 1281.
(2) Zaera, F. *Prog. Surf. Sci.* **2001**, *69*, 1.
(3) Antczak, G.; Ehrlich, G. *Surf. Sci. Rep.* **2007**, *62*, 39.
(4) Lin, N.; Dmitriev, A.; Weckesser, J.; Barth, J. V.; Kern, K. *Angew. Chem., Int. Ed.* **2002**, *41*, 4779.
(5) Maksymovych, P.; Sorescu, D. C.; Dougherty, D.; Yates, J. T. *J. Phys. Chem. B* **2005**, *109*, 22463.
(6) Stipe, B. C.; Rezaei, M. A.; Ho, W. *Science* **1998**, *279*, 1907.
(7) Rao, B. V.; Kwon, K. Y.; Liu, A. W.; Bartels, L. *J. Chem. Phys.* **2003**, *119*, 10879.
(8) Lauhon, L. J.; Ho, W. *J. Chem. Phys.* **1999**, *111*, 5633.
(9) Sheppard, N.; Mathieu, M. V.; Yates, D. J. C. *Z. Elektrochem.* **1960**, *64*, 734.
(10) Beebe, T. P.; Crowell, J. E.; Yates, J. T. *J. Chem. Phys.* **1990**, *92*, 5119.
(11) Lee, J. G.; Ahner, J.; Mocuta, D.; Denev, S.; Yates, J. T. *J. Chem. Phys.* **2000**, *112*, 3351.
(12) Gao, Q.; Dohnalek, Z.; Cheng, C. C.; Choyke, W. J.; Yates, J. T. *Surf. Sci.* **1994**, *312*, 261.
(13) Yates, J. T.; Alvey, M. D.; Dresser, M. J.; Henderson, M. A.; Kiskinova, M.; Ramsier, R. D.; Szabo, A. *Science* **1992**, *255*, 1397.
(14) Fujishima, A.; Zhang, X. T.; Tryk, D. A. *Surf. Sci. Rep.* **2008**, *63*, 515.
(15) Diebold, U. *Surf. Sci. Rep.* **2003**, *48*, 53.
(16) Zhang, Z.; Bondarchuk, O.; Kay, B. D.; White, J. M.; Dohnalek, Z. *J. Phys. Chem. C* **2007**, *111*, 3021.
(17) Zhang, Z.; Bondarchuk, O.; White, J. M.; Kay, B. D.; Dohnalek, Z. *J. Am. Chem. Soc.* **2006**, *128*, 4198.
(18) Zhang, Z. R.; Rousseau, R.; Gong, J. L.; Li, S. C.; Kay, B. D.; Ge, Q. F.; Dohnalek, Z. *Phys. Rev. Lett.* **2008**, *101*, 156103.

 10.1021/ja907431s

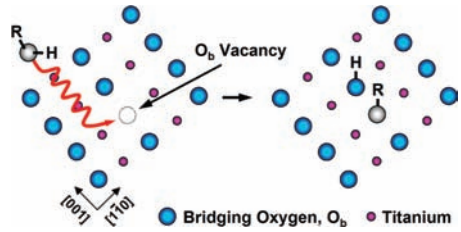

Figure 1. Schematic view of alcohol (ROH) dissociation on O_b vacancy (O_V) of TiO_2(110).

of the hydrocarbon group dynamics. We find that the alkyl chains preferentially sit on the neighboring Ti^{4+} rows in an orientation that depends on the position of the hydroxyl group within the octanol. At 300 K, the alkyl chains readily rotate between energetically equivalent positions. For isolated 2-, 3-, and 4-octoxy species, rotational motion across the O_b row becomes frozen upon cooling to 150 K. When the octoxy is nascently paired with its hydroxyl group, cross-O_b-row rotation occurs between two inequivalent configurations, a less favorable one with the H−CO hydrogen facing the HO_b and a more favorable one with the H−CO_b hydrogen facing away.

2. Experimental Section

The experiments were performed in an ultrahigh-vacuum chamber (base pressure $<8 \times 10^{-11}$ Torr) equipped with a variable-temperature STM (Omicron), an Auger electron spectrometer (AES), and a quadrupole mass spectrometer (QMS). The TiO_2(110) sample ($10 \times 3 \times 0.5$ mm^3, Princeton Scientific) was mounted on a modified Omicron double-plate sample holder which allowed for sample heating and cooling. The heating power dependence on sample temperature was calibrated in a separate experiment using a TiO_2(110) crystal with a chromel−alumel (type K) thermocouple glued directly to the crystal surface. The TiO_2(110) was cleaned by repeated cycles of Ne^+ sputtering and annealing up to 900−950 K. AES was used to determine the presence of impurities on the sample surface. The concentration of O_V's on the surface was 7−9%. 1-, 2-, 3-octanol (Sigma-Aldrich, ≥ 97%) and 4-octanol (Fluka, ≥ 98%) were purified by several freeze−pump−thaw cycles using liquid nitrogen and dosed on TiO_2(110) at 300 K in the STM stage via a retractable tube doser.[19] All STM images (empty states) were collected using a constant current (∼0.1 nA) tunneling mode with a positive sample bias voltage (empty states, ∼1.0 V) and processed using WSxM software (Nanotech, freeware).[20] Further details about the experimental system and sample preparation were described previously.[19,21]

3. Computational Details

Calculations were carried out employing density functional theory (DFT) with a gradient-corrected functional for exchange and correlation[22] as implemented in the CP2K package.[23,24] Core electrons are modeled as norm-conserving pseudopotentials.[25] The wave functions were expanded in a molecularly optimized double-zeta Gaussian basis set to minimize basis set superposition errors,[26] which is required for reliable calculation of weak intermolecular interactions. An additional auxiliary plane wave basis of 300 Ry energy cutoff was used for the calculation of the electrostatic energy terms. Dispersion forces, typically not well modeled by gradient-corrected functionals, are included by the DFT-D method of Grimme,[27] where an attractive C_6 dispersion coefficient and the corresponding cutoff function are added to the DFT potential to account for dispersion at long range. For this approximation we used the standard parameter set of Grimme[27] without any parameter optimization and an interaction cutoff of 7 Å. All surface reactions are modeled on a (6×3) rutile TiO_2(110) surface slab of four TiO_2 units depth and a 12 Å thick vacuum layer to minimize electrostatic interactions between periodic images in the direction of the surface normal. Finally, the Γ-point approximation was employed for Brilluoin zone integration.

As a test of our approximations, specifically with respect to our treatment of van der Waals (vdW) interactions, we calculated desorption energies of a series of physisorbed *n*-alkanes on the rutile TiO_2(110) surface. These molecules represent a good test system for modeling of the vdW interactions of the alkyl chains of the octoxy species as described in the following section. For these species the largest component of the attraction arises from the C−Ti 3.6−4.5 Å close contacts because C and Ti are the most polarizable atoms in the molecule and surface, respectively. This leads to desorption energies of 21, 37, 49, and 85 kJ/mol for ethane, propane, butane, and octane, respectively. These values compare fairly well with the binding energies of 34, 46, 58, and 97 kJ/mol obtained from TPD spectra of these alkanes on TiO_2(110) (not shown). The TPD analysis was carried out using a previously described procedure developed in our group and employed for the analysis of alkanes from other surfaces.[28−30] It is noted that, without the vdW interactions, the binding energies of the alkanes to the surface are found to be 1−8 kJ/mol, indicating that spurious weak interactions arising from the overlap term at long distances for GGA functionals have only a minor effect on the binding energies.

4. Results and Discussion

4.1. Room-Temperature Dynamics. Figure 2 displays STM images of TiO_2(110) after exposure to 1-, 2-, 3-, and 4-octanol at 300 K. The TiO_2(110) exhibits alternating rows of low-lying Ti^{4+} (bright) and high-lying O_b's (dark) running diagonally from upper-left to bottom-right.[15] The distance between adjacent O_b atoms is 2.95 Å, and that between neighboring O_b rows is 6.5 Å. On the basis of our previous studies of shorter alcohols,[16,17] the bright features centered on the O_b rows are assigned to alkoxy species formed via alcohol dissociation on the O_V sites, RO−H + O_V + O_b → R−O_b + H−O_b, as schematically shown in Figure 1. Upon alcohol dissociation on O_V's, a hydroxyl group is formed on an adjacent O_b site of the same O_b row.[16,17] For the octanols, these hydroxyl species cannot be resolved due to the large size of the octoxy species. Although hydroxyls are not directly observed here, their existence is indirectly confirmed by the experiments that are discussed further below. Two of the few remaining O_V sites (faint features on the dark O_b rows) are marked in Figure 2a.

Interestingly, instead of the single bright, elongated lobe expected for the alkyl chain of a static 1-octoxy species (Figure

(19) Zhang, Z.; Bondarchuk, O.; Kay, B. D.; White, J. M.; Dohnalek, Z. *J. Phys. Chem. B* **2006**, *110*, 21840.
(20) Horcas, I.; Fernandez, R.; Gomez-Rodriguez, J. M.; Colchero, J.; Gomez-Herrero, J.; Baro, A. M. *Rev. Sci. Instrum.* **2007**, *78*, 013705.
(21) Li, S. C.; Zhang, Z.; Sheppard, D.; Kay, B. D.; White, J. M.; Du, Y.; Lyubinetsky, I.; Henkelman, G.; Dohnalek, Z. *J. Am. Chem. Soc.* **2008**, *130*, 9080.
(22) Perdew, J. P.; Burke, K.; Ernzerhof, M. *Phys. Rev. Lett.* **1996**, *77*, 3865.
(23) Lippert, G.; Hutter, J.; Parrinello, M. *Mol. Phys.* **1997**, *92*, 477.
(24) VandeVondele, J.; Krack, M.; Mohamed, F.; Parrinello, M.; Chassaing, T.; Hutter, J. *Comput. Phys. Commun.* **2005**, *167*, 103.
(25) Goedecker, S.; Teter, M.; Hutter, J. *Phys. Rev. B* **1996**, *54*, 1703.
(26) VandeVondele, J.; Hutter, J. *J. Chem. Phys.* **2007**, *127*, 114105.
(27) Grimme, S. *J. Comput. Chem.* **2006**, *27*, 1787.
(28) Tait, S. L.; Dohnalek, Z.; Campbell, C. T.; Kay, B. D. *J. Chem. Phys.* **2006**, *125*, 234308.
(29) Tait, S. L.; Dohnálek, Z.; Campbell, C. T.; Kay, B. D. *J. Chem. Phys.* **2005**, *122*, 164707.
(30) Tait, S. L.; Dohnálek, Z.; Campbell, C. T.; Kay, B. D. *J. Chem. Phys.* **2005**, *122*, 164708.

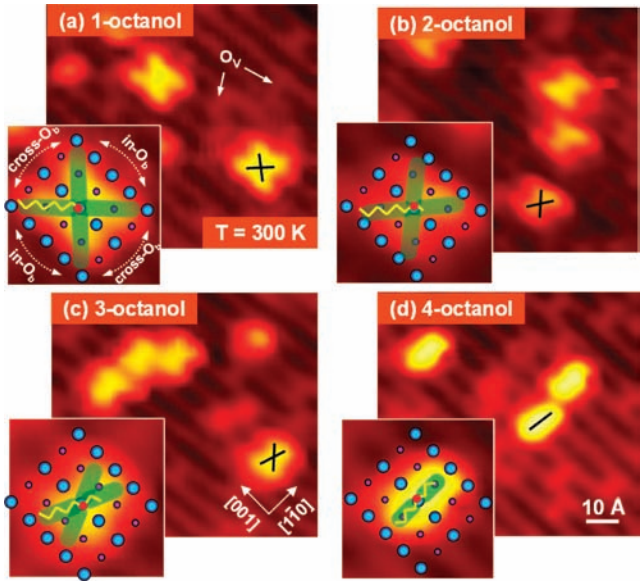

Figure 2. STM images of partially reduced TiO_2(110) after adsorption of (a) 1-, (b) 2-, (c) 3-, and (d) 4-octanol at 300 K. The insets show magnified areas with the octoxy species overlaid by TiO_2(110) ball models (O_b, blue; Ti^{4+}, magenta). The yellow zigzag lines shows the alkyl chains, and red dots mark the anchoring position on the O_b row. Green lobes forming an "X" shape for 1-, 2-, and 3-octoxy and an "I" shape for 4-octoxy indicate how fast rotation of the octoxy species leads to the formation of such features in the STM images. In all cases, the coverages were kept very low ($<2 \times 10^{13}$ molecules/cm^2) to isolate the alkoxy species from each other. While not observable in the STM images, the geminate HO_b species are present next to most of the octoxy species (see text).

2a), we observe a bright X-shaped feature centered above the original position of an O_V, with four lobes stretching into the neighboring Ti^{4+} rows. This X-shaped structure arises from alkyl chain rotation between four equivalent local energy minima around the anchoring C$-$$O_b$ bond with a rate that is fast compared to the slow STM acquisition rate. Hence, the acquired image represents a time average of the alkoxy species in these four positions, as schematically illustrated in the ball model inset in Figure 2a. Measurement of the length of a single lobe within the X feature yields ~8 Å, which is very close to the length of a 1-octoxy chain (O_b-C_8 = 9 Å), further supporting our explanation.

This interpretation is further corroborated by considering how the situation is altered when considering the interactions of other octanol isomers, namely 2-, 3-, and 4-octanol, with the TiO_2(110) surface. As shown in Figure 2b,c, 2- and 3-octoxy also appear as X's, indicating that they also rotate rapidly around the anchoring C$-$$O_b$ group between four equivalent local energy minima on the surface. Upon closer inspection, a small degree of asymmetry in the X's can be seen for some of the 2- and 3-octoxy species. While the exact origin of such asymmetry is unclear, it is likely that it results from perturbations caused by the local environment (e.g., neighboring O_V's or HO_b's). Nonetheless, a clear trend can be seen moving from 1- to 2- to 3-octanol, with the length of a single lobe within the X feature decreasing from ~8 Å for 1-octanol to ~7 Å and ~6 Å for 2- and 3-octanol, respectively. These lengths compare favorably with the lengths of the longer chains from the anchoring C$-$$O_b$ bond, e.g., C_2-C_8 = 7.5 Å for 2-octoxy and C_3-C_8 = 6.3 Å for 3-octoxy. Additionally, from 1-octanol to 2- and 3-octanol, the distance between the ends of the lobes on the same Ti^{4+} row decreases, indicating that as the length of the longer alkyl chain from the C$-$$O_b$ anchor gets smaller, the lowest energy

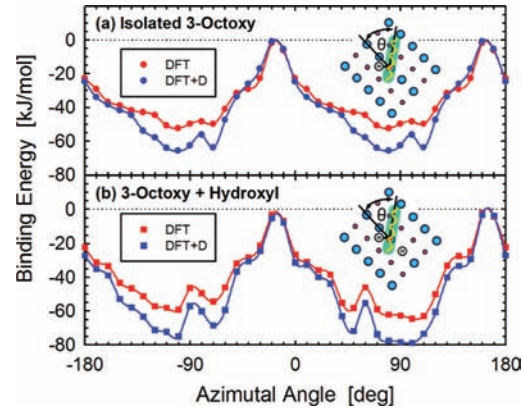

Figure 3. Calculated torsional potential for the rotation of the isolated 3-octoxy species about the anchoring C$-$$O_b$ bond: (a) isolated 3-octoxy and (b) 3-octoxy in the presence of a geminate HO_b group. The azimuthal angle, θ, is defined as the angle between the O_b row and the largest moment of inertia of the hydrocarbon chain (top and bottom insets). Torsional potentials were calculated using DFT (red data points) and DFT-D (blue data points).

orientation becomes closer to perpendicular to the O_b row ([1$\bar{1}$0] direction). This trend is completed for 4-octanol, Figure 2d, where instead of an X, an I-shaped feature perpendicular to the O_b row is observed. Here the length of the lobe (5.5 Å) is slightly larger than the length of the longer part of the alkyl chain (C_4-C_8 = 5.0 Å). The same perpendicular orientation was observed for short alkyl chains of 2-butoxy.[16] While the STM images do not allow us to directly determine whether the 4-octoxy is stationary or rotating between two equivalent positions, the hindered rotations observed for 1-, 2-, and 3-octoxy species strongly suggest rapid rotation. This conclusion is further supported by theoretical calculations discussed below.

To understand these observations at a molecular level, we have undertaken a computational mapping of the torsional potential for the rotation of the isolated 3-octoxy group about the C$-$$O_b$ bond. For these calculations we constrained the $O_b-C_3-C_8$ plane to have a fixed angle with respect to the plane of the O_b row and relaxed all other variables. From this we extract a torsional angle, θ, which is defined as the angle between the O_b row and the unit vector of the longest moment of inertia of the carbon chain; see schematic in Figure 3a. The calculated energy landscape (blue circles) shows 4 minima at $\theta = -100°$, $-70°$, 80°, and 110°; note that the asymmetry in the torsional potential results from the fact that the zigzag nature of the conformations in the alkyl chain have a lower symmetry than the underlying C_{2v} point group of the TiO_2(110) surface. Examining the geometry of the optimized structures at these minima, it is observed that these orientations provide approximately 2$-$3 Ti$-$C contact distances between 4.0$-$5.0 Å, slightly longer than those observed for the physisorbed alkanes (see section 4.3). The four minima are separated by two different types of barriers: a small barrier of 9$-$10 kJ/mol at $\theta = -80°$ and 100° and a larger barrier of 65 kJ/mol at $\theta = -20°$ and 160°. Thus, our theoretical calculations corroborate the conclusion that the X shape observed from the STM measurements results from the presence of four minima which are in part stabilized by close Ti$-$C vdW contacts.

To further probe the electronic origin of these two barriers, we also include the torsional potential calculated without the dispersion component (Figure 3a, red circles). The shape of the potential with and without dispersion is identical around the maximum of the highest barrier, whereas the two curves

deviate markedly in shape and well depth around the potential minima, with a noted decrease of over 6 kJ/mol in the potential barriers at $\theta = -80°$ and 100°. This result can be understood in the following manner. The larger potential maximum at the transition state for rotation of the alkyl chain across the O_b row arises from the largely repulsive interactions due to the short distance (~3.0 Å) of C_{1-2} and C_{4-5} carbon atoms (neighbors of the anchoring C_3-O_b) from the O_b row. Within the DFT-D model this repulsive term is modeled by Pauli repulsion in the DFT functional, with negligible stabilizing influences from the dispersion term. On the other hand, in the region of the potential minimum, the additional dispersion from Ti−C interactions adds approximately 15 kJ/mol extra stabilization relative to DFT alone. In addition, the enhanced corrugations of the potential within the potential valleys around $\theta = -130°$ to $-50°$ and 60° to 130° largely arise from the dispersion term, specifically from the ability to maximize Ti−C interactions at $\theta = -100°$, $-70°$, 80°, and 110°. Thus, our theoretical calculations suggest that the observed X shape from the STM measurements results in the presence of four minima which are stabilized by close Ti−C vdW contacts, whereas the barriers for rotation across the O_b row are dominated by steric repulsion.

We also consider the calculated torsional potential in the presence of a geminate HO_b, as shown in Figure 3b. In general the potential retains the same shape as that observed for the isolated 3-octoxy. Two large barriers of about 72 kJ/mol are observed at −15° and 165° for the rotation across the O_b row and two small barriers at −90° and 60° of 15−20 kJ/mol, leading to four well-resolved minima; note that the presence of the adjacent HO_b group further breaks the symmetry of the structure relative to that of the carbon chain alone (Figure 3a), leading to a completely asymmetric potential. It is noted that the two minima above 0° in Figure 3b are shifted by about 10° and the well depth/barrier heights are increased when compared to those of isolated 3-octoxy (Figure 3a). This is a result of the larger repulsions between the geminate HO_b group and the alkyl chain, as discussed in more detail below in the context of examining the low-temperature STM images. This scenario is more representative of the experimentally observed images in Figure 2c, where majority of the 3-octoxy species are present as geminate pairs with HO_b's.[16,17]

Based on the trends observed in Figures 2 and 3, several conclusions can be made about the interactions of the alkyl chains with the underlying TiO_2(110). In all cases the alkyl chains are located on top of Ti^{4+} sites and minimize overlap with the O_b rows, in accord with our understanding of the factors governing the energetics for the 3-octoxy potential energy surface. To test that this hypothesis can explain the trends in the observed conformations of the alkyl chains, we performed short simulated annealing trajectories where the octoxy chains of 1-, 2-, 3-, and 4-octoxy are relaxed from a configuration equilibrated at $T = 300$ to 0 K in 1−2 ps. We find that the minima for 1-, 2-, 3-, and 4-octoxy respectively have the longer carbon chain oriented at $\theta = 40°$, 55°, 70°, and 90° relative to the O_b row, resulting in 3−5 Ti−C contacts on the order of 3.5−4.5 Å. This is in good accord with the experimentally observed trend of $\theta = 34°$, 40°, 56°, and 90° for the same species, respectively.

We conclude that the observed conformations of the octoxy chains are guided by maximizing the number of C−Ti vdW contacts while minimizing C···O repulsive ones. This is not surprising, since the attractive interactions for the alkyl groups are primarily based on dispersion forces that are stronger on

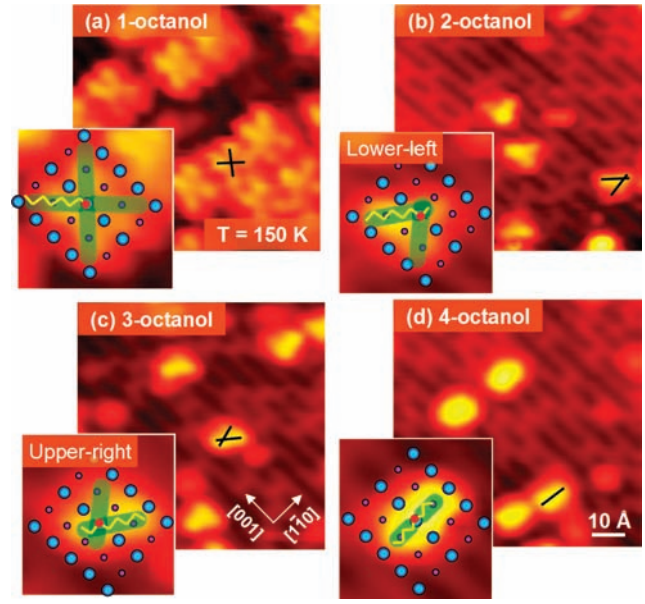

Figure 4. STM images of partially reduced TiO_2(110) after adsorption of (a) 1-octanol, (b) 2-octanol, (c) 3-octanol, and (d) 4-octanol at 300 K and imaging at 150 K. The legend to the insets is described in Figure 2. While not observable in the STM images, the geminate HO_b species are present next to most of the octoxy species (see text).

Ti^{4+} than on O_b sites. This has been shown previously on TiO_2(110) for the case of other weakly bound species such as N_2, O_2, CO.[31] As the alkyl chains get longer, a tilt from the orientation perpendicular to the O_b rows is used to accommodate the whole chain on the Ti^{4+} rows.

4.2. Low-Temperature Dynamics. The observation of X-shaped features for octoxy species at room temperature and multiple minima calculated on the potential energy surface show that the octoxy species rapidly rotate about the $C-O_b$ and spend about the same amount of time among the nearly equivalent positions. Direct evidence for the rotation of the octoxy species was obtained by acquiring STM images at 150 K. While the 1-octoxy species remain X-shaped (Figure 4a), dramatic changes can be seen in the appearance of 2- and 3-octoxy species (Figure 4b,c). Their images become V-shaped, with equal fractions pointing to the lower-left and upper-right Ti^{4+} rows next to the anchoring O_b row. This observation indicates that the rotation of 2- and 3-octoxy across the O_b rows is frozen and therefore the species rotate only between the two equivalent positions within the same Ti^{4+} row, as illustrated by the ball models (insets in Figure 4b,c). This clearly shows that for 2- and 3-octanol the barrier for cross-O_b-row rotation is larger than that for in-O_b-row rotation. While initially one would expect that the intensities of both lobes in V shapes would be the same, in most cases one lobe appears brighter than the other in the STM images. We believe that this asymmetry originates from the asymmetry of the two potential energy minima in the torsional potential, as shown in Figure 3.

The observed conversion of X to V shape corresponds well with the barrier we obtain from theoretical calculations (Figure 3). Rotation between sites on the same side of the O_b row is relatively facile at 150 K, with a theoretically predicted barrier of ~10 kJ/mol. This barrier is sufficiently low for transitions between minima to be observed but high enough that the

(31) Dohnalek, Z.; Kim, J.; Bondarchuk, O.; White, J. M.; Kay, B. D. *J. Phys. Chem. B* **2006**, *110*, 6229.

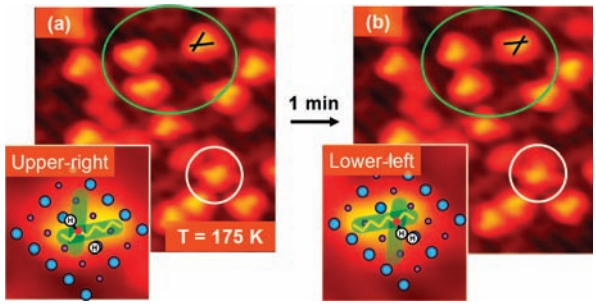

Figure 5. Two subsequent STM images (1 min apart) obtained at 175 K on TiO_2(110) after 3-octanol adsorption and dissociation on O_V sites at 300 K. The images illustrate switching of the 3-octoxy species across the O_b row. The legend to the insets is described in Figure 2.

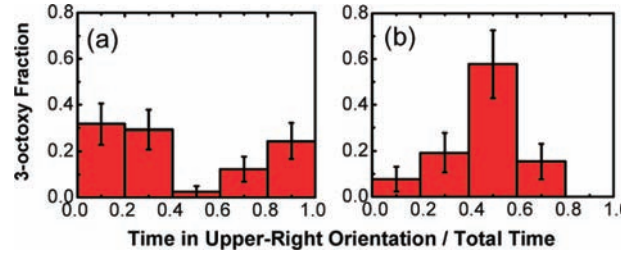

Figure 6. Distribution of fractional time that 3-octoxy species spend in the upper-right Ti^{4+} row with respect to the anchoring O_b row: (a) as adsorbed at 300 K, imaged at 175 K, and (b) preannealed to 400 K, imaged at 160 K.

population at the transition state is low, leaving two well-resolved density maxima in the STM image. The cross-row diffusion barriers for the isolated 3-alkoxy and 3-alkoxy-HO_b geminate pair were calculated to be 65 and 72 kJ/mol, respectively, and hence this motion is highly improbable.

Additionally, since the cross-O_b-row rotation has not been frozen at 150 K for 1-octoxy, we conclude that the cross-O_b-row barrier for 1-octoxy is smaller than those for 2- and 3-octoxy. This is further supported by cross-row rotational barriers of 25, 49, 65, and 62 kJ/mol calculated for isolated 1-, 2-, 3-, and 4-octoxy species, respectively, using DFT-D. The trends in the calculated barriers can be rationalized simply in terms of the number and length of the alkyl chains attached to the carbon atom that is anchored to the O_b row. As already discussed for the case of 3-octoxy (discussion of Figure 3), the potential barrier for cross-O_b-row rotation arises primarily from repulsive interactions due to the short distance of C_{1-2} and C_{4-5} carbons from the O_b row (~3.0 Å) at the transition state. Based on the same reasoning, a very similar barrier is also predicted for 4-octoxy cross-row rotation. In contrast, a significantly lower barrier is expected for 1-octoxy where only carbons, C_{2-3}, of a single chain are within a short distance from the O_b row. The 2-octoxy species is an intermediate case with one chain being a short methyl group. In this case, the steric hindrance due to proximity of CH_3- with the neighboring O_b is smaller than for the longer chains, leading to only a moderate increase in the barrier as compared to 1-octoxy.

4.3. Interactions of Alkyl Groups with Geminate Hydroxyl. To further explore the rotation barrier of the alkoxy groups across the O_b row, we have dosed 3-octanol at 300 K and cooled to 175 K to allow for a slow rotation of the alkyl chains between the two adjacent Ti^{4+} rows. Two subsequent STM images demonstrating the hindered cross-O_b-row rotation of 3-octoxy species at 175 K are shown in Figure 5. Within 1 min, three 3-octoxy species highlighted by green ovals switched their orientation with respect to the anchoring O_b row. This is further illustrated by the ball models shown in the insets of Figure 5.

While we expected that the probability of 3-octoxy species in the upper-right and lower-left configuration would be the same, the STM movie (Supporting Information) clearly shows that 3-octoxy species have a strong preference for spending most of the time on one side of the O_b row (some oriented to upper-right, others to lower-left). After switching to the unfavorable orientation, 3-octoxy species quickly switch back to the favored one. To quantify this preference we have evaluated a number of 3-octoxy species (~50) and determined the fraction of time they spend in the upper-right orientation. The results are plotted as a histogram in Figure 6a. Statistically, 95% of the species show a strong preference for spending a larger fraction of time in one of two configurations of the O_b row (some oriented to upper-right, others to lower-left). (Hypothetically, if half of the species would spend 100% of the time in the upper-right configuration and the other half in the lower-left configuration, only two bars would be observed in Figure 6a, one centered at 0.1 and the other at 0.9, both with fraction of 0.5.) We have further determined the average hopping rates from and to the favorable configuration to be 4×10^{-3} and 2×10^{-2} s^{-1}, respectively.[21] The symmetric appearance of the distribution in Figure 6a clearly shows that the rotation across the O_b rows is unaffected by the STM tip. Since the tip scans are carried out only in one direction (e.g., left to right), any tip-induced rotational motion would manifest itself in a distribution skewed toward one direction (lower-left or upper-right). The same argument also applies to Figure 6b that is discussed below.

While the isolated O_b-bonded 3-octoxy species does not provide a source of orientation preference, the neighboring hydroxyl group resulting from the alcohol dissociation does. This is schematically shown in the ball model insets in Figure 5. In one orientation, the hydrogen bonded to the anchoring C atom (H−CO) points toward the neighboring HO_b, while in the other it faces away.

As already mentioned, the hydroxyls in the octoxy/hydroxyl pairs cannot be resolved due to the size of the octoxy species. Nonetheless, direct confirmation of the influence of neighboring hydroxyl on the orientation preference of 3-octoxy species is obtained by annealing the 3-octanol exposed TiO_2(110) to 400 K before cooling to 175 K and imaging the dynamics of the 3-octoxy groups. Based on our prior studies,[21] annealing to 400 K leads to facile hydrogen diffusion, enabling the neighboring hydroxyls to move away from the 3-octoxy species. Interestingly, after the 400 K annealing most of the 3-octoxy species (~70%) show a fuzzy X shape (data not shown) at 175 K instead of the expected V shape. This suggests that the isolated 3-octoxy species (after hydrogen has diffused away) have a lower cross-O_b-row rotation barrier than in the presence of neighboring HO_b, as already indicated by the DFT-D calculation presented in Figure 3.

A small fraction of fuzzy X features was also observed at 175 K without preannealing. An example of such a fuzzy X-shaped feature is marked by the white circles in Figure 5. The presence of these features without annealing suggests that a few of the initial hydroxyl−octoxy pairs have already separated during the 300 K 3-octanol dose. This observation is consistent with our prior studies, where the diffusion of hydroxyl hydrogens away from the initial alkoxy−hydroxy pairs was also observed. We have shown that this process is mediated by mobile, undissociated Ti^{4+}-bound alcohol molecules before they find a vacant O_V site.[16,17]

To slow down the cross-O_b-row rotation of isolated 3-octoxy species, we cooled the 400 K annealed sample to 160 K. At this temperature the rate of cross-O_b-row rotation is slower than the STM scanning rate, and therefore repeated imaging of the same area can be used to determine whether there is an orientation preference similar to that determined in Figure 6a. The results shown in Figure 6b clearly demonstrate that, in the absence of a neighboring HO_b, the majority of the 3-octoxy species sample both configurations (upper-right and lower-left) with equal probability without any apparent orientational preference. (Hypothetically, if all species would spend exactly 50% of the time in each configuration, a single bar with fraction of 1.0 centered at 0.5 would be observed.) The difference in the 3-octoxy rotational motion in the presence and/or absence of the HO_b neighbors is clearly evident in the STM movies (Supporting Information) acquired before and after surface annealing. The average rate of O_b-row crossing in the absence of HO_b neighbors at 160 K is determined to be 3×10^{-3} s^{-1}. This value can be used to estimate the cross-O_b-row rotational barrier. Assuming the rotation process is Arrhenius-like, the rotation rate is given as $\nu = \nu_0 \exp(-\Delta E/RT)$, where ν_0 is the attempt frequency, ΔE the activation energy, R the universal gas constant, and T the temperature. Assuming a typical attempt frequency of $\sim 10^{13}$ s^{-1}, we obtain a cross-O_b-row rotation barrier of 47 kJ/mol (which is lower than our theoretical estimate by about 18 kJ/mol). A similar estimate of the cross-O_b-row rotational barriers in the presence of neighboring HO_b can be made on the basis of the switching rates of 2×10^{-2} s^{-1} into and 4×10^{-3} s^{-1} out of the favorable orientation determined at 175 K. The resulting barriers are 49 and 52 kJ/mol for the rotation into and out of the favorable configuration, respectively. Values of both barriers in the presence of HO_b are higher than that of isolated 3-butoxy, suggesting that the increased corrugation of the O_b row with an adjacent hydrogen atom leads to a slight increase ($\sim$2−5 kJ/mol) in the cross-O_b-row rotation barrier. Additionally, the steric repulsion between neighboring hydrogens of the HO_b and the H−CO_b (inset of Figure 5b) leads to the lower stability of this configuration with respect to the one where H−CO_b and H−O_b hydrogens are apart (inset of Figure 5a) by $\sim$3 kJ/mol.

In general, the scenario observed for rotational dynamics obtained from our STM measurements and the underlying energy barriers are in good qualitative accord with our theoretical estimates. The observed experimental barrier for 3-octoxy cross-row diffusion of 47 kJ/mol is less than the 65 kJ/mol obtained by our theoretical estimate, which is not surprising given the approximate nature of the DFT-D approach. However, the trend in the barrier height for cross-row rotation in the presence of a geminate HO_b group is also born out by our theoretical estimates. The additional repulsion arising from H−C nonbonded contacts of 2.1−2.5 Å at the transition state between the HO_b and C_{1-2} and C_{4-5} carbons of the alkyl chain was found to increase the barrier to 72 kJ/mol, as shown in Figure 3.

By comparing the torsional potential with and without a geminate HO_b group, much insight can be gained into how the dynamics of the alkoxy rotation is altered when the H−O_b hydrogen is in the near vicinity of the alkyl chain. As already noted, the net barrier to rotate across the O_b row is slightly higher by about 10 kJ/mol. This can be ascribed entirely to repulsion, as the difference between the curves with and without vdW interactions is affected to the same extent when HO_b is not present. Interestingly enough, the barrier between the minima on the same side of the O_b row is also increased (by about 5 kJ/mol). This can be traced to an increase in the repulsion at the transition state due to short CH···HO_b contacts on the order of about 2.3 Å; note that the barrier for rotation between the minima at 100° and 70°, as well as the one at −100° and −70°, is still present without the vdW interactions, unlike when HO_b is not present. In addition, the increased steric hindrance caused by the HO_b group leads to a slight energetic asymmetry between the two minima on the same side of the O_b row; the minima at ±70° are about 6 kJ/mol destabilized with respect to those at ±100°. Finally, it is noted that the locations of the minima are also slightly shifted by $\sim$10° between the potential with and without hydroxyls, indicating that repulsion with the HO_b group may also slightly shift the observed orientations.

Both our theoretical and experimental analyses indicate that, in the presence of a neighboring hydroxyl group, the rotational potential and subsequent dynamics become mildly retarded, as well as more asymmetric due to the increased steric repulsions between the alkane chain and the hydoxyl group.

5. Conclusions

In summary, we present the first STM study of the rotational dynamics of an organic species, octoxy, on an oxide surface, TiO_2(110). The octoxy species together with the bridging hydroxyls (HO_b) form as a result of octanol dissociation on the bridging oxygen (O_b) vacancy (O_V) defect sites. The STM images obtained at 150 and 300 K show that the alkyl chains of the octoxy species are positioned on the Ti^{4+} rows (neighboring the anchoring O_b row), where the attractive dispersion forces are maximized. The exact orientation of the alkyl chain depends on the position of the anchor (C−O_b), as determined by the original position of OH in 1-, 2-, 3-, and 4-octanol. For isolated octoxy species, two rotational barriers are present, a small one for motion within the same Ti^{4+} row and a larger one for motion across the O_b row. In the presence of neighboring HO_b, the cross-O_b-row rotation of the octoxy leads to two structurally and energetically inequivalent configurations, a less favorable one with the H−CO hydrogen facing the HO_b and a more favorable one with the H−CO hydrogen facing away from the HO_b. The combination of atomistic simulation and our STM measurements has evolved a picture wherein the observed alkyl chain orientations are found to be stabilized by Ti···C vdW interactions which lead to a corrugated potential energy surfaces, with a resulting static and dynamic disorder among multiple binding configurations.

While the role of translational diffusion of adsorbed species in catalytic reactions is well recognized (e.g., bringing the reagents together and/or to the catalytically active site), the role of rotational motion is generally not acknowledged. Nonetheless, arguments similar to those put forward for translational diffusion (e.g., positioning the reagent in the right spatial configuration to undergo reaction) apply also to the rotational motion. For example, the rotation dynamics of alkoxy species is expected to couple into the alcohol dehydration on TiO_2(110). In this reaction, the alkoxy species undergo β-hydride elimination involving simultaneous cleavage of the C−O_b and β-C−H bonds as a rate-limiting step.[32,33] In the transition state, the alkyl chain is likely aligned with the O_b row to facilitate β-C−H cleavage and deposition of the H atom on the O_b site. As such, the relative

(32) Bondarchuk, O.; Kim, Y. K.; White, J. M.; Kim, J.; Kay, B. D.; Dohnalek, Z. *J. Phys. Chem. C* **2007**, *111*, 11059.
(33) Kim, Y. K.; Kay, B. D.; White, J. M.; Dohnalek, Z. *Catal. Lett.* **2007**, *119*, 1.

time that the alkoxy species spends in this configuration vs its more favored orientations could directly affect the rate of the dehydration reaction.

Acknowledgment. This work was supported by the U.S. Department of Energy Office of Basic Energy Sciences, Division of Chemical Sciences, Biosciences and Geosciences, and performed at W. R. Wiley Environmental Molecular Science Laboratory, a national scientific user facility sponsored by the Department of Energy's Office of Biological and Environmental Research located at Pacific Northwest National Laboratory (PNNL). PNNL is operated for the U.S. DOE by Battelle Memorial Institute under Contract No. DE-AC06-76RLO 1830.

Supporting Information Available: Two isothermal STM movies illustrating the rotational dynamics of 3-octoxy on TiO_2(110) in the presence (S1) and in the absence (S2) of the geminate HO_b species. This material is available free of charge via the Internet at http://pubs.acs.org.

JA907431S